Stress Effects in Ferroelectric Thin Films*

L. Lian and N.R. Sottos
Department of Theoretical and Applied Mechanics
University of Illinois Urbana-Champaign
Urbana, IL 61801

Abstract

Ferroelectric thin films develop large residual stresses and preferred crystallographic orientation during processing which can effect electromechanical properties and performance. The present work investigates the effects of stress on field-induced polarization switching in ferroelectric PZT (52/48) thin films. Film response is measured as a function of externally applied mechanical stress using a double-beam laser-Doppler heterodyne interferometer. This apparatus successfully eliminates any displacement contribution from flexural vibration of the substrate and enables measurement of the strain-electric field hysteresis loops as a function of applied stress. The field-induced strain in the PZT film increases with increasing compressive stress, while the opposite trend is observed for applied tensile stress. The dependence of electromechanical response on the external stress is attributed to the initial tensile residual stress state in the film. Tensile stress creates an in-plane clamping effect on the domains in the film, hindering polarization switching. The application of a compressive stress reduces tensile residual stress in the film and the constraint on the domains; hence more 90° polarization switches are allowed to occur under applied electric field, leading to higher field-induced strains. Applied tensile stress amplifies the clamping effect, leading to lower field-induced strains. Experimental observations are consistent with numerical simulations based on existing micromechanical models of polarization switching.

* Submitted for publication in the *Journal of the Mechanics and Physics of Solids* (2001).

1. Introduction

Ferroelectric films were developed in the early 1960s to extend electromechanical transducers to higher frequencies (Foster, 1964). Interest in the processing and properties of ferroelectric thin films has continued to grow during the past three decades. Compared with their bulk counterparts, thin film ferroelectric ceramics have several advantages for use as active elements in electromechanical devices. One of the most important advantages is small inertia mass, which enables higher cut-off frequencies and wider operational bandwidths for electromechanical devices and makes ferroelectric thin films promising for high-frequency transducer applications. Another key advantage of ferroelectric thin films is the large energy density that can be achieved due to high dielectric strength. Breakdown strengths on the order of 10^8 V/m have been reported (Li *et al.*, 1993). As a result, the films are desirable for micro-sensors, micro-actuators and ultrasonic motors (Morney *et al.*, 1989, Wenzel *et al.*, 1988, Polla *et al.*, 1986). A third advantage of ferroelectric thin films is the low driving voltage and relatively rapid speed of polarization switching for use in nonvolatile random-access memory and switching capacitors for integrated circuitry (Frey *et al.*, 1993, Bondurant *et al.*, 1989). Additionally, new types of ferroelectric thin films that can achieve switching strains approaching 1% are in development. Among the many families of ferroelectrics, perovskite $Pb(Zr_xTi_{1-x})O_3$ (or PZT) thin films are the most extensively fabricated and used due to their remarkable ferroelectric, piezoelectric, and pyroelectric properties, especially when the composition is near the morphotropic phase boundary (x~0.5).

Several different deposition methods have been used to prepare ferroelectric thin films, including chemical vapor deposition (Nakagawa *et al.*, 1982), sputtering deposition (Surowiak *et al.*, 1978), sol-gel techniques (Budd *et al.*, 1985), and laser ablation deposition (Kidoh *et al.*, 1991). Sol-gel processing is the most popular deposition method since it is relatively inexpensive and compatible with a wide variety of substrate materials. A typical sol-gel deposition includes four steps. First, a precursor solution is prepared according to compositional requirements. Next, the precursor solution is cast onto a substrate (usually Si) spinning at approximately 3000 rpm. The film and substrate are then heat treated after each layer is deposited to remove volatile organic species. Finally, after several layers are deposited, the substrate and the piezoelectric layers are fired at high temperature (usually above 600°C) to promote densification and crystallization.

Since the fabrication of ferroelectric thin films involves growth of the film on a substrate of different material and high temperature treatment, significant residual stress develops in the film after processing. The total residual stress in the polycrystalline film consists of intrinsic and extrinsic contributions. The intrinsic stress is induced by shrinkage and constrained densification during drying and firing, formation of intergranular stresses as anisotropic grains grow and by structural transformations at the Curie temperature. Extrinsic thermal stresses are induced upon

cooling due to the mismatch between the developing thermoelastic properties of the film with those of the substrate, while further extrinsic stress originates from the lattice parameter mismatch between the film and the substrate. Residual stresses on the order of several hundred MPa have been reported for various ferroelectric thin films (Sengupta *et al.*, 1998, Lappalainen *et al.*, 1997, Spierings *et al.*, 1995, Ong, 2001).

Several researchers have attributed changes in ferroelectric film structure and properties to the residual stress state. Tuttle *et al.* (1992) reported that the sign of the film stress at the Curie point controls the orientation of the domain structure and thus, the switchable spontaneous polarization and strain in PZT thin films. Compressive stresses upon cooling through the Curie point resulted in domains with their *c*-direction and polarization vector normal to the film surface, while tensile stresses induced domains with their *a*-direction normal to the surface and with polarization vector in the plane. As a result, PZT films deposited on sapphire under compressive residual stress exhibited superior ferroelectric properties as compared to films deposited on silicon substrates under tensile residual stress. Kweon *et al.* (1997) also found that the *c*-axis orientation ratio was related to the intrinsic stress generated during deposition of lead titanate films.

Reduction in the residual stress state due to annealing has led to measurable changes in the poling direction and switching behavior of PZT films (Spierings *et al.*, 1995). Lappalainen *et al.* (1997) have also reported an increase in dielectric constant and a decrease in coercive field with decreasing residual stress for Nd-modified PZT films. Garino and Harrington (1992) studied residual stress effects in sol-gel derived PZT films on platinized Si wafers. Tensile residual stresses of several hundred MPa were measured. The influence of these stresses on ferroelectric properties was ascertained through electrical measurements on a film with and without the application of an external mechanical stress. Decreasing the tensile residual stress in the film by ~30% was found to increase the remanent polarization by ~11% and the dielectric constant by ~2%.

More recently, Lian and Sottos (2000) reported significant changes in the properties of PZT thin films with different thickness and crystallographic orientation. The measured piezoelectric constants, field-induced strains and dielectric constants all decreased with diminishing film thickness. In addition, films with (100) preferred orientation had higher piezoelectric coefficients, smaller loss factors, and higher saturation and remnant polarizations than films with (111) preferred orientation. The thickness and crystallographic orientation dependence of the electromechanical properties was attributed to the residual stress state in the film, which is also dependent on thickness and processing conditions.

In bulk ferroelectric ceramics, applied compressive stress is known to have a significant effect on electromechanical behavior. Cao and Evans (1993) investigated the stress-induced depolarization in poled hard and soft PZT. The strain and depolarization were measured

continuously while uniaxial compressive stress was applied either parallel or perpendicular to the poling direction of a compression cuboid. Both materials were nonlinear when the stress in the poling direction exceeded ~20 MPa, and exhibited permanent deformations (~0.5%) and residual depolarization (~80%) after exposure to stresses above 500 MPa. Lynch (1996, 1998) measured strain-electric field and polarization-electric field hysteresis loops of PLZT and PZT at various compressive stress levels. Both the field-induced strain and field-induced polarization decreased significantly as the compressive stress parallel to the electric field was increased. The significant effects of applied stress observed in bulk ferroelectric ceramics provide strong evidence for the possibility of stress induced switching behavior in ferroelectric thin films under high levels of residual stress.

The present work investigates the influence of applied stress on field-induced polarization switching in ferroelectric PZT (52/48) [$Pb(Zr_{0.52}Ti_{0.48})O_3$] thin films. The field-induced strain in the film is measured using laser interferometry while an external stress is applied by bending the substrate.

2. Constitutive Behavior

Ferroelectricity is defined as the reversibility of the direction of the electric dipole in a polar crystal by means of an applied electric field and can occur only in the 10 pyroelectric crystal classes that contain a unique polar axis (an electric dipole moment) in the unstrained condition (Jaffe, 1971). Many ferroelectric ceramics, such as $BaTiO_3$, and $Pb(Zr,Ti)O_3$, crystallize in the perovskite structure. The unit cell of an ABO_3 perovskite type oxide is shown schematically in Fig. 1 to illustrate the typical ferroelectric switching process. The ABO_3 perovskite structure contains an A cation at each corner, a B cation in the body center and an O^{2-} anion at the center of each face of the unit cell. The coordination numbers of A and B are 8 and 6, respectively. At temperatures above the Curie point, the unit cell is cubic symmetric, has no polar axis, and therefore is not ferroelectric (Fig. 1a). If the temperature drops to a level below the Curie point, phase transformation occurs and the unit cell spontaneously changes to a tetragonal, orthorhombic, or rhombohedral shape, depending on material and composition state and becomes polar (only the tetragonal unit cell is shown in Fig. 1b). Relative displacement of the positive and negative ions results in a dipole moment and spontaneous strain. The dipole moment per unit volume is the polarization. The coupling between strain, polarization, stress, and electric field is a consequence of this polar structure.

Under small loads, the polarization and strain of the unit cell undergo reversible changes proportional to the applied electric field or stress. These linear effects are the direct and converse piezoelectric effects. If the electric field in a direction other than that of the current polarization exceeds the coercive field, the central ion moves to another of the six off-center

tetragonal sites (Fig. 1b). This field results in a change of the polarization direction to one most closely aligned with the electric field and a change in the direction of the spontaneous strain associated with the polar axis. A similar phenomenon occurs if stress larger than the coercive stress is applied to the unit cell. However, only 90° (70.5° or 109.5° in the rhombohedral structure) polarization switching can be induced by applied stress (Fig. 1c). This phenomenon is called ferroelastic switching. Ferroelectric and ferroelastic polarization switching together with linear elastic and piezoelectric effects are the source of the unique constitutive behavior of ferroelectrics, which can be expressed as

$$\varepsilon_{ij} = s^{E}_{ijkl}\sigma_{kl} + d_{kij}E_k + \varepsilon^{R}_{ij} \tag{1}$$

$$D_i = d_{ikl}\sigma_{kl} + \kappa^{\sigma}_{ik}E_k + P^{R}_{i} \tag{2}$$

where ε_{ij}, D_i, σ_{kl}, E_k, s^{E}_{ijkl}, d_{kij} and κ^{σ}_{ik} are the total strain tensor, the total electric displacement vector, the mechanical stress tensor, the electric field vector, the elastic compliance tensor, the piezoelectric tensor and the dielectric permittivity tensor, respectively. The terms ε^{R}_{ij} and P^{R}_{i} are the remanent strain and polarization caused by polarization switching, and are obtained upon removal of electrical and mechanical loading, respectively.

A ferroelectric ceramic is an agglomeration of small single crystals that consist of many unit cells. As the temperature cools through the Curie point, the unit cell deforms, usually with a lengthening in the direction of the polar axis. Since each unit cell has its own polarization direction, a high-energy state occurs due to the incompatibility of the spontaneous strain and polarization between neighboring unit cells. The total energy within each single crystal or grain is minimized by the formation of domains, which are regions that have common orientation of the spontaneous dipole. Adjacent domains are separated by domain walls. The formation of domains also results in small average strain and polarization in each grain and minimizes intergranular incompatibility and stresses. When an electric field above the coercive field is applied to the ceramic, ferroelectric switching occurs. This switching results in domain wall movement and incompatible strains and polarizations. Domain wall motion is an energy dissipating process due to anharmonic lattice interactions and pinning defects such as dopant ions and vacancies.

Constitutive models to describe the nonlinear response of ferroelectric ceramics can be classified into two broad groups. One group is based on general thermodynamic theory and the second is based on micromechanical behavior of grains. Bassiouny *et al.* (1988 a, b, c, and d) have developed a thermodynamic framework for coupled electromechanical hysteresis effects using internal variable theory. Electric polarization is chosen as the internal variable and the dissipation inequality is decomposed into a rate independent and a rate dependent part. The free energy function is expanded into third order polynomial in strain and polarization to include

nonlinear effects such as electrostriction. Bassiouny's theory is capable of predicting electromechanical hysteresis effects and mechanical and electrical "hardening" in continuous ferroelectric media. Kamlah *et al.* (1997) also report a macroscopic constitutive model based on internal variable theory that is able to predict butterfly hysteresis (strain vs. electric field) and dielectric hysteresis (polarization vs. electric field) behavior as well as the effects of uniaxial stress, but is limited to one-dimensional loading. Since the thermodynamic based models are phenomenological in nature, they are not able to account for microstructure such as grain size and orientation effects.

In the second group of models based on the microscopic behavior of the grains, each crystallite is represented as a spherical inclusion in an infinite homogeneous matrix with average properties of the ceramic. Polarization switching of an individual grain is considered the source of the classic butterfly shaped strain versus electric field curves and the corresponding electric displacement versus electric field loops. If the electrical and mechanical energy reduction of each grain exceeds a critical energy barrier, then switching occurs. The macroscopic behavior is controlled by the combination of the average microscopic switching behavior and the reversible linear behavior. In the model proposed by Hwang *et al.* (1995), the polarization and strain for an individual grain are predicted from the applied electric field and stress through a Preisach hysteresis model (Macki *et al.*, 1993). The response of the bulk ceramic to applied loads is predicted by averaging the response of individual grains with random orientation. This model has been modified to include additional terms that account for the interaction of local granular strains and polarizations with the volume average polarization of the ceramic (Lynch *et al.*, 1995, Hwang *et al.*, 1998a and b), saturation of the linear piezoelectric effect, structural change between tetragonal and rhombohedral, and phase transformation between anti-ferroelectric and ferroelectric phases (Chen *et al.*, 1998a and b). The additional terms help give a better representation of real material behavior.

Hwang and McMeeking (1998b and c) have also developed a finite element model of switching in polycrystalline ferroelectric ceramics. In the simulation, each crystallite is represented by a cubic finite element with the crystallographic principle direction of each crystallite assigned randomly. The model assumes a crystallite switches if the reduction in potential energy of the system exceeds a critical energy barrier per unit volume of switching material. In all of the models discussed above, domains are assumed to switch completely between distinct states of strain and polarization. However, experimental observations indicate a single crystal switches by progressive movement of domain walls. Huber *et al.* (1999) have developed a constitutive model drawing upon self-consistent crystal plasticity theory to predict the progressive switching of each crystal. This model is able to capture the qualitative features of ferroelectric switching, such as butterfly and dielectric hysteresis loops. Due to the theoretical complexity, the model is not straightforward to implement and no quantitative comparison with experimental has been reported to date.

The micro-electro-mechanical model of Hwang *et al.* (1998a and b) captures the nonlinearities and hysteresis associated with the orientation distribution of the grains. In particular, it is able to predict the characteristic dielectric hysteresis in the electric displacement versus electric field response and 'butterfly' hysteresis in the strain versus electric field curve. Chen and Lynch (1998a) successfully implemented this model to simulate the depolarization effect of compressive stress and ferroelastic response in bulk 8/35/65 PLZT. Predictions were in close agreement with experimental values. In the current work, this model is applied to interpret the in-plane stress effects in ferroelectric thin films.

3. Stress Effect on Beam Deflection

Measuring the effect of stress on the field-induced strain in a ferroelectric thin film is challenging due to the planar geometry and small out-of-plane displacements. Traditional piezoelectric measurement techniques such as the resonance method and the strain gage method used for bulk ferroelectrics are not suitable for films. In addition, the experimental set-up must allow for the application of an external stress and direct measurement of the deformation of the film. Several high-resolution interferometric techniques have been adopted for characterizing thin-film response. Li *et al.* (1994, 1995, 1996) constructed a single-beam Michelson interferometer to study the electromechanical coupling of a variety of ferroelectric thin films over a wide range of frequencies. Kholkin *et al.* (1996) used a modified Mach-Zender interferometer to investigate the electric field, frequency and time dependent piezoelectric response of PZT thin films. While Michelson and Mach-Zehnder interferometers have high resolutions, both are sensitive to the surrounding environment and require significant effort to align the laser beams and stabilize the working point. Lian and Sottos (2000) developed a robust, laser-Doppler heterodyne interferometric technique to quantify changes in the d_{33} piezoelectric coefficients and field-induced strains of rigidly mounted PZT thin films. This single beam interferometric method was used initially in the current study to measure field-induced displacements in films subjected to applied stress.

PZT thin film samples were obtained from NZ Applied Technologies (Wolburn, MA) with a Zr/Ti ratio of 52/48. The films were deposited on platinized silicon wafer substrates using the sol-gel technique and cut into rectangular beams. The crystallization behavior of these films was examined at room temperature by x-ray diffraction and the microstructure was evaluated by scanning electron microscopy (Lian and Sottos, 2000). Samples tested in the current study had well aligned columnar grains with a preferred (100) orientation.

Stress effects were investigated by applying a static bending load to the film and substrate using the apparatus shown in Fig. 2. One end of the beam sample is clamped onto a mirror mount, which can be manually adjusted for angular tilt when aligning the interferometer. A load

cell (Sensotec, Model 31/1426-03) attached to a translation stage, which moves perpendicularly with respect to the sample surface measures the force applied at the free end of the cantilever beam. The amount of force applied is controlled by the position of the translation stage. A high performance process indicator (OMEGA, Model DP41-S) supplies the excitation voltage to the load cell and displays the output from it.

The single-beam laser Doppler heterodyne interferometer described in Lian and Sottos (2000) is used to measure the deflection of the entire beam sample under different compressive stress levels. A schematic of the beam sample used in the interferometric measurements is shown in Fig. 3. Gold electrodes of 1 mm in diameter are evaporation-deposited onto the top surface of the PZT film through a shadow mask. A portion of the PZT layer at the corner is etched away to leave the Pt layer exposed for the bottom electrode. Electric contacts are made to the top and bottom electrodes with fine copper wires of 0.001" in diameter. Prior to any interferometric measurements, a static point force is applied at the end of the cantilever beam sample by adjusting the position of the translation stage. The uniaxial stress in the PZT film due to bending of the substrate is calculated using beam theory. The interferometer is then carefully aligned and the portion of the unpoled film between the bottom and top electrodes is driven by a large sinusoidal 1.0 kHz ac electric field. During the experiment, the sample is translated horizontally at a speed of 5 μm/s while the lock-in amplifier recorded amplitude of the out-of-plane velocity at each point on the scan across the film surface. After the displacement data are recorded, the magnitude of the static point force is changed and the interferometric measurement repeated.

A plot of the beam displacement as a function of applied load is shown in Fig. 4. A significant increase in displacement due to excitation of the film is observed for increasing values of applied compressive stress. The measured beam displacements are large compared to the film displacements reported in Lian and Sottos (2000). While the cantilever mounting method enables the application of an external load, it also allows flexural deflection of the substrate when the ferroelectric film is activated. Without a rigid back mount, the entire beam is excited by the small portion of the film under the electrode. Nevertheless, the vibration of the beam is due solely to the deformation of the film induced by applied electric field and the displacement data in Fig. 4 indicate that the response of the film depends significantly on the applied stress.

As discussed in the Introduction, the residual stress in PZT films deposited on platinized Si substrate has been measured previously by several researchers (Garino *et al.* 1992, Spierings *et al.* 1995, Lappalainen *et al.*, 1997, and Ong 2001) and found to be tensile with a magnitude greater than 100 MPa . Although the residual stress was not measured directly for the films tested, the experiments reported previously by Ong (2001) and others indicate that the PZT (52/48) films investigated in the current project are in a state of residual tension. Although the

initial residual stress state in the film is biaxial, the application of biaxial stress is prohibitive due to the beam-like sample geometry. As a result, only the residual stress in the longitudinal direction of the beam is relieved or intensified during the bending experiment. The increased displacement response with the application of compressive stress in Fig. 4 is attributed to the relief of residual tensile stress in the film.

4. Double-beam Heterodyne Interferometer

The deflection of the beam must be eliminated from the experimental measurements to explicitly investigate stress effects on film response. A double-beam interferometer in which the probing beam reflects from both the front and back surfaces of the sample (Fig. 5) was constructed by modifying the single beam heterodyne interferometer configuration reported in Lian and Sottos (2000). The bending contribution of the substrate is removed by the exact cancellation of the optical path-length change of the two beams impinging on the sample. This type of interferometer was first described by Zhang *et al.* (1989) for strain measurements in bulk ferroelectric materials and later was modified to measure the response of piezoelectric thin films by Kholkin *et al.* (1996).

The full optical arrangement of the double-beam Doppler heterodyne interferometer is shown in Fig. 6. A single frequency, linearly polarized laser beam of wavelength 514.5 nm from an argon laser (Lexel Laser model 3500) is incident upon a 40 MHz acousto-optic modulator (AOM) producing two beams which are sent along different arms of the interferometer. One beam is shifted in frequency by 40 MHz and used as a reference beam. The other beam, which has the same frequency as the beam incident upon the AOM, is directed to the back side of the substrate first and then reflected to the front surface of the film and sharply focused at normal incidence onto a point just opposite to the probing point on the other side. The $\lambda/2$ plate is used to rotate the polarization vectors of the sample and reference beams to the horizontal direction. The combination of the polarizing beam splitters and the quarter-wave plates in the probing arm of the interferometer reduces the light loss of the sample beam. The convex lenses L-1 and L-2 have the same focal lengths. They are mounted onto translation stages and their positions are carefully adjusted so that the reflecting surfaces of the sample are exactly in the focal planes of the lenses.

In order to completely eliminate the substrate bending effect, the laser beams hitting the back and front surfaces of the sample must be colinear. By placing a partial reflective mirror in the position of the sample and then carefully adjusting the tilt angle and position of the polarized beam splitter (PB-2) and lens (L-2), the laser beams passing through and reflected back from the partial reflective mirror can be aligned on top of each other. The reference and sample beams are recombined at the nonpolarizing beam splitter. The resulting interference pattern at the surface

of the photodetector produces a voltage proportional to the intensity of light focused on it. The frequency of the interference signal received by the photodetector is equal to 40 MHz plus or minus the instantaneous Doppler frequency shift. The principle of operation and instrumentation of this double-beam interferometer is the same as that described in Lian and Sottos (2000) for the single-beam Doppler heterodyne interferometer except that an oscilloscope (Tektronix, TDS 420) is used instead of the lock-in amplifier to measure the transient field-induced strains in the PZT film.

As for the single beam interferometric measurements, a static point force was first applied to the end of the cantilever beam sample by adjusting the position of the translation stage. The double-beam interferometer was carefully aligned so that sample beam was focused onto the center of the top electrode. The portion of the unpoled film between the bottom and top electrodes was then driven by a large sinusoidal 1.0 kHz AC electric field. An averaging function of the digital oscilloscope was used to acquire the signal from the vibrometer controller. The time-dependent out-of-plane deformation of the film was obtained by integrating the output signal of the oscilloscope with respect to time. After the data was recorded, the magnitude of the static point force was changed and the interferometric measurement was repeated at the same point on the film surface.

5. Results and Discussion

The film chosen for the double-beam interferometric measurement was 1.6 μm thick with a (100) preferred orientation. The width, length and thickness of the beam were 9 mm, 60 mm and 0.38 mm, respectively. The displacement profile in the vicinity of the activated top electrode was measured first with no applied stress to ensure the bending contribution of the substrate was completely eliminated. The amplitude and frequency of the driving voltage applied were 20 volts (peak to peak) and 1.0 kHz, respectively. The displacement quickly diminished outside the electroded areas indicating that the bending contribution of the substrate was successfully subtracted from the measurement by using the double-beam interferometric technique.

Typical butterfly-type strain hysteresis loops are shown in Fig. 7a for the PZT film under increasing compressive bending load. Each loop represents an average of 10,000 cycles. As the external compressive stress in the film increased from zero to -48 MPa, the field-induced strain increased about 18%. In addition, strain hysterisis loops were measured for the PZT film under increasing tensile bending load (Fig. 7b). As the external tensile stress in the film increased from zero to 44 MPa, the field-induced strain decreased about 26%.

To gain further insight into the experimental observations, the micro-electro-mechanical model developed by Hwang *et al.* (1998) was used to simulate the response of a representative tetragonal ferroelectric ceramic subject to biaxial in-plane stress and electric field. The

theoretical formulation and numerical implementation of this model are summarized in the Appendix. Because all of the electromechanical properties of the ferroelectric thin films are not well characterized and expected to be quite different from that of bulk material with the same composition, only a qualitative comparison can be made with experiments. Notwithstanding this, the numerical simulation offers physical insight into the polarization switching process under general states of stress and electric field.

The microstructure and behavior of lead zirconate titanate (PZT) is closely related to its composition. The unit cell changes from orthorhombic, rhombohedral to tetragonal as the mole % of $PbZrO_3$ decreases from 100 to 0. Since the model of Hwang *et al.* (1998) assumes tetragonal unit cells and the PZT film investigated in the current work has a composition of 52/48, data for a PZT that has tetragonal unit cells and a composition equal or close to 52/48 is desired for the numerical simulation. Experimental data reported by Saito and Hori (1994) on bulk, polycrystalline tetragonal 53/47 PZT are chosen for the numerical simulation to extract material constants and parameters. The values of all relevant model parameters are listed in Table 1.

The transverse biaxial tensile stress effect on the electro-mechancial behavior of 53/47 PZT with preferred orientation is predicted using the numerical procedure summarized in the Appendix. Biaxial tensile stress in the plane perpendicular to the electric field is gradually introduced and held fixed after reaching a certain value. An electric field is then introduced and cycled between the positive and negative limits. Fig. 8 contains longitudinal strain versus electric field hysteresis loops for increasing values of transverse, biaxial tensile stress. Both the shape and magnitude of the field-induced strain hysteresis loops change significantly with the application of stress. The in-plane stress creates a clamping effect that prevents 90^0 polarization switching in alignment with the electric field and decreases the overall field-induced strain. This result is similar to the effect of compressive stress applied parallel to the poling field reported by Lynch (1998) for bulk PZT. The field-induced strain loops measured for the thin films in Fig. 7 lack a sharp turn-around at the peak field and are qualitatively more similar to the curves predicted under biaxial loading. Fig. 9 shows the longitudinal strain versus electric field hysteresis loops under biaxial tensile stress as the magnitude of stress in one direction is reduced, while the other is held constant (similar to the bending experiments). The reduction of the tensile stress leads to an increase of the field-induced strain and electric displacement. These results are also in qualitative agreement with the thin film response reported in Fig. 7.

Both the results of the bending experiments and the model simulations indicate that the initial tensile residual stress state in the films creates an in-plane clamping effect on the domains. The application of a compressive stress relieves the tensile residual stress in the film and the constraint on the domains, hence more 90° polarization switches are allowed to occur under applied electric field, which leads to higher field-induced strains (Fig. 7a). On the other hand,

the application of tensile stress amplifies the clamping effect, which leads to decreased field-induced strains in the film as the external stress increases (Fig. 7b).

Residual stress effects appear to play a critical role in determining the properties and performance of ferroelectric thin film structures. These effects will become even more dominant as the characteristic length scale of film devices becomes smaller and smaller. Ong (2001) recently reported that the residual stress in PZT films processed by the sol gel technique increases significantly with diminishing film thickness. Changes in the residual stress state with film thickness are likely to be the primary cause of the dramatic decrease in field-induced strains with decreasing film thickness measured by Lian and Sottos (2000). Integration of electroceramic thin films is a critical technology for the realization of future microelectromechanical (MEM) device applications such as miniaturized sensors and actuators, ultrasonic motors and optical elements as well as nonvolatile memory and switching capacitors for integrated circuitry. A key issue is the ability to rapidly pattern films into fine-scale architectures without degrading properties or performance characteristics. Understanding the effects of residual stresses developed during processing on film properties and how to tailor these stresses for optimal device performance is essential to advance this technology for the next generation of electromechanical devices.

6. Conclusions

PZT (52/48) film response was measured as a function of externally applied mechanical stress using laser-Doppler heterodyne interferometry. Mechanical stress was applied by static beam bending, and the displacement profile of the film/substrate beam was measured with a single beam interferometer. The displacement of the beam was found to increase as the applied uniaxial compressive stress in the PZT film increased. A unique double-beam laser-Doppler interferometer was built to isolate the electric field response of the film from that of the vibration of the substrate. Application of a compressive bending stress to relieve the tensile residual stress in PZT (52/48) film increased the field-induced strains. The opposite effect was observed for application of a tensile stress. Experimental observations are consistent with numerical simulations based on existing micromechanical models of polarization switching. Overall, these results indicate that the initial residual stress state in the film has a significant influence on electromechanical performance of the film.

Acknowledgements

This work was supported by the National Science Foundation under grant NSF CMS 00-88206. The authors would like to acknowledge helpful conversations with Professor David Payne and Mr. Ryan Ong in the Department of Material Science and Engineering at the University of Illinois at Urbana-Champaign.

Appendix

The micro-electro-mechanical model developed by Hwang *et al.* (1998a and b) considers the ferroelectric ceramic as an aggregation of many randomly oriented grains. The crystal structure of each grain is assumed tetragonal as shown in Fig. 1 (rhombohedral structure is not considered). Each crystallite obeys the constitutive law described by eqs. (1) and (2). Inhomogeneities in the local electric and stress fields are ignored so that each crystallite is subjected to the same loading condition. All material properties are assumed to be uniform in each crystallite but can differ from that of other crystallites. A global Cartesian coordinate system is fixed in space and all components of vectors and tensors in eqs. (1) and (2) are referred to the global coordinate system.

In order to simplify the simulation, the crystallite is modeled as elastically and dielectrically isotropic, and κ and s are given by

$$\kappa_{ij} = \kappa\delta_{ij} \tag{3}$$

$$s_{ijkl} = \frac{1+\nu}{Y}\delta_{ik}\delta_{jl} - \frac{\nu}{Y}\delta_{ij}\delta_{kl} \tag{4}$$

where δ is the Kronecker delta, Y is the Young's modulus, ν is the Poisson's ratio, and κ is the dielectric permittivity. The piezoelectric coefficient tensor for each crystallite is also simplified and considered as transversely isotropic. The nonzero components include d_{333}, d_{311}, d_{113},, d_{322} and d_{223} and it is assumed that

$$d_{311} = d_{322} = -\frac{1}{2}d_{333} \tag{5}$$

when referred to a crystallite coordinate system in which the positive x_3-axis is parallel to the positive polarization direction.

The principle values of the spontaneous strain of each grain are aligned with the local coordinates and have the values of $e_o = c_o - a_o / a_o$ in the direction parallel to the polarization and the values of $e_o = -2(a - a_o)/a_o$ in the direction perpendicular to the polarization, where c and a correspond to the lengths of the tetragonal unit cell, and a_0 is the lattice parameter of a

reference cubic cell with the same volume. The magnitude of the spontaneous polarization is P_0 and is directed along the *c*-axis.

A crystallite is assumed to switch when the reduction of potential energy of the system due to that switch exceeds a critical value, which can be considered as the energy barrier that must be overcome to achieve the switch. The switching criterion is expressed as

$$-\Delta U \geq V_c \psi_c \tag{6}$$

where ΔU is the change of potential energy due to the switch, V_c is the volume of the switching crystallite and ψ_c is the energy barrier against the switch per unit volume. To estimate the change of potential energy for a switch, the individual crystallite is treated as a switching spherical inclusion embedded in a homogeneous matrix with a fixed remanent strain ε^{rm} and polarization P^{rm}. The potential energy of such an inclusion is approximated as that of a spherical isotropic elastic inclusion with a transformation strain in a homogeneous isotropic elastic matrix with a different residual strain plus the energy of an isotropic electrostatic inclusion with a spontaneous polarization in an isotropic matrix with a different remanent polarization. McMeeking and Hwang (1997) have shown that the switching criterion can be written as

$$\alpha(\sigma_{ij} + \frac{2}{5}\bar{Y}\varepsilon_{ij}^{rm})\Delta\varepsilon_{ij}^{ri} + (E_i + \frac{1}{3\bar{\kappa}}P_i^{rm})\Delta P_i^{ri} \geq 2\bar{E}_0 P_0 \tag{7}$$

where α is a weighting parameter differentiating the mechanical energy and the electrical energy in driving switching, $\bar{Y}$ is an effective modulus, and $\bar{\kappa}$ is an effective dielectric permittivity. The values for α, $\bar{Y}$, $\bar{\kappa}$ and $\bar{E}_0$ are chosen to provide the best fit to experimental data, and the value of $\bar{E}_0$ for 90^0 switching ($\bar{E}_0^{90}$) and 180^0 switching ($\bar{E}_0^{180}$) can be different. The macroscopic response of the ceramic is computed from the volume average response of each crystallite. The strain and polarization of each crystallite are computed according to eqs. (1) and (2) in the local coordinate system and then rotated to the global system and averaged.

The thin films tested in the current work have a preferred (100) orientation. Theoretical investigations of orientation effect are scarce since most of the work to date has focused on the characterization of bulk ferroelectric ceramics, which have no preferred orientation. The Hwang *et al.* (1998) micromechanical model does allow for the selection of crystallographic orientation on the unit cell level, and thus makes it possible to incorporate the orientation effect. Each crystallite has its own three tetragonal axes defined by three Euler angles in Fig. 10. The orientation of the local coordinate system relative to the global coordinate system is defined as $x_j = a_{ji}X_i$ where a_{ji} are the direction cosines between the local and the global coordinate system and the subscripts refer to Cartesian coordinate directions. A spontaneous polarization of magnitude P_0 is assigned randomly to one of the two directions parallel to the *c*-axis of the tetragonal unit cell and the spontaneous strain is e_0 in the *c*-axis direction and $-e_0/2$ in the other

two principle directions. In the case of a ceramic with (100) preferred orientation, the three Euler angles are generated by the random number generator in MATLAB in such a way that ϕ has a normal distribution with a mean of $\pi/2$ and a variance of $\pi/10$, θ is uniformly distributed between 0 and 2π, and ψ has a normal distribution with a mean of 0, $\pi/2$, $3\pi/2$ or π and a variance of $\pi/10$.

Numerical simulation starts with input of the numbers of crystallites and incremental steps. Based on preliminary simulations performed on sets of 1000, 2000, 3000, 5000, and 7500 crystallites, an aggregation of 5000 crystallites (an effective compromise between reproducibility and computing time) is chosen for the calculations presented in Section 5. During a simulation, the load (electrical or mechanical or both) are gradually introduced so that only a few crystallites can switch at a given stage. After a small increment of load is made, each crystallite is checked to see if it has met the switching criterion given by eqn (7). The tetragonal symmetry dictates six possible switches for each crystallite and the switch associated with the greatest value of the left hand side of eqn (7) is taken to occur. After all possible switches have been identified and made, the macroscopic remanent strain and polarization are computed by averaging over all crystallites. With $\boldsymbol{P}^{rm}$ and ε^{rm} updated, further switching is allowed to occur without increase of the load. This process is repeated until no more crystallites will switch. The linear contribution to the strain and electric displacement is then computed for each crystallite from the linear terms in eqns (1) and (2), with eqns (3) and (4) used for the elastic compliance and dielectric permittivity tensor. The macroscopic electric displacement and strain are then calculated as the volume average of that in the crystallite.

References

Bassiouny, E. and Maugin, G.A., 1988a. Thermodynamical formulation for coupled electromechanical hysteresis effects - I. Basic equations. *International Journal of Engineering Science* **26** (12): 1279-1295.

Bassiouny, E. and Maugin, G.A., 1988b. Thermodynamical formulation for coupled electromechanical hysteresis effects - II. Poling of ceramics. *International Journal of Engineering Science* **26** (12): 1297-1306.

Bassiouny, E. and Maugin, G.A., 1989a. Thermodynamical formulation for coupled electromechanical hysteresis effects - III. Parameter identification. *International Journal of Engineering Science* **27** (8): 975-987.

Bassiouny, E. and G. A. Maugin, G.A., 1989b. Thermodynamical formulation for coupled electromechanical hysteresis effects - IV. Combined electromechanical loading. *International Journal of Engineering Science* **27** (8): 989-1000.

Bondurant, D. and Gnadinger, F., 1989. Ferroelectrics for nonvolatile RAMs. *IEEE Spectrum* **26** (7): 30-33.

Budd, K. D., Dey, S. K. and Payne, D.A., 1985. Sol-gel processing of $PbTiO_3$, $PbZrO_3$, PZT, and PLZT thin films. *British Ceramic Proceedings* **36**: 107-121.

Cao, H. and Evans, A. G., 1993. Nonlinear deformation of ferroelectric ceramics. *Journal of American Ceramic Society* **76** (4): 890-896.

Chen, W. and Lynch, C. S., 1998a. A micro-electro-mechanical model for polarization switching of ferroelectric materials. *Acta Materialia.* **46** (15): 5303-5311.

Chen, W. and Lynch, C. S., 1998b. A model for simulating polarization switching and AF-F phase changes in ferroelectric ceramics. *Journal of Intelligent Material Systerms and Structures* **9**: 427-431.

Foster, N. F., 1964. Ultra-high frequency cadmium-sulphide transducers. *IEEE Transactions on Sonics and Ultrasonics* **11**: 63-68.

Frey, M. H. and Payne, D. A., 1993. Nanocrystalline barium titanate: evidence for the absence of ferroelectricity in sol-gel derived thin-layer capacitors. *Applied Physics Letters* **63** (20): 2753-2755.

Garino, T. J. and Harrington, H. M., 1992. Residual stress in PZT thin films and its effect on ferroelectric properties. *Material Research Society Symposium Proceedings* **243**: 341-347.

Huber, J. E., Fleck, N. A., Landis, C. M. and McMeeking, R. M., 1999. A constitutive model for ferroelectric polycrystals. *Journal of the Mechanics and Physics of Solids* **47**: 1663-1697.

Hwang, S. C., Lynch, C. S. and McMeeking, R. M., 1995. Ferroelectric/ferroelastic interactions and a polarization switching model. *Acta Metallurgica et Materialia* **43** (5): 2073-2084.

Hwang, S. C. and McMeeking, R. M., 1998a. The prediction of switching in polycrystalline ferroelectric ceramics. *Ferroelectrics* **207**: 465-495.

Hwang, S. C., Huber, J. E., McMeeking, R. M. and Fleck, N. A., 1998b. The simulation of switching in polycrystalline ferroelectric ceramic, *Journal of Applied Physics* **84** (3): 1530-1540.

Hwang, S. C. and McMeeking, R. M., 1998c. A finite element model of ferroelectric polycrystals. *Ferroelectrics* **211**: 177-194.

Hwang, S. C. and McMeeking, R. M., 1999. A finite element model of ferroelastic polycrystals. *International Journal of Solids and Structures* **36**: 1541-1556.

Jaffe, B. 1971. *Piezoelectric Ceramics*. New York: Academic Press Inc.

Kamlah, M., Bohle, U., Munz, D. and Tsakmakis, C., 1997. Macroscopic description of the nonlinear electro-mechanical coupling in ferroelectrics, *Smart Structures and Materials 1997: Mathematics and control in Smart Structures,* SPIE, **3039**: 144-155.

Kidoh, H., Ogawa, T., Yashima, H., Morimoto, A. and Shimizu, T., 1991. Influence of laser fluence on structural and ferroelectric properties of lead-zirconate-titanate thin films prepared by laser ablation. *Japanese Journal of Applied Physics Part 1-Regular Papers Short Notes & Review Papers*, **30** (9B): 2167-2169.

Kholkin, A., Wütchrich, C., Taylor, D. V. and Setter, N., 1996. Interferometric measurements of electric field-induced displacements in piezoelectric thin films. *Review of Scientific Instruments*, **67** (5): 1935-1941.

Kweon, S.Y, Yi, S.H. and Choi, S.K., 1997. Intrinsic stress dependence of c-axis orientation ratio in $PbTiO_3$ films deposited by reactive sputtering. *J. Vac. Sci. Technol.* A, **15** (1) 57-61.

Lappalainen, J., Frantti, J. and Lantto, V., 1997. Electrical and mechanical properties of ferroelectric thin-films laser ablated from a $Pb_{0.97}Nd_{0.02}(Zr_{0.55}Ti_{0.45})O_3$ target. *Journal of Applied Physics* **82** (7): 3469-3477.

Li, J.-F., Viehland, D. D., Tani, T., Lakeman, C. D. E. and Payne, D. A., 1993. Piezoelectric properties of sol-gel-derived ferroelectric and antiferroelectric thin layers, *Journal of Applied Physics* **75** (1): 442-448.

Li, J.-F., Viehland, D. D., Tani, T., Lakeman, C. D. E. and Payne, D. A., 1994. Piezoelectric properties of sol-gel-derived ferroelectric and antiferroelectric thin layers. *Journal of Applied Physics* **75** (1): 442-448.

Li, J.-F., Viehland, D. D., Tani, T., Lakeman, C. D. E. and Payne, D. A., 1995. Frequency-dependent electromechanical properties for sol-gel deposited ferroelectric lead zirconate titanate thin layers: Thickness and processing effects. *Journal of Materials Research* **10** (6): 1435-1440.

Li, J.-F. and Viehland, D. D., 1996. The nonlinear, complex, induced-piezoelectric response of Pb(Mg/sub 1/3/Nb/sub 2/3/)O/sub 3/-PbTiO/sub 3/ relaxors. *Journal of Applied Physics* **80** (6): 3451-3456.

Lynch, C. S., Hwang, S. C. and McMeeking, R. M., 1995. Micromechanical Theory of the non-linear Behavior of Ferroelectric Ceramics. *Active Materials and Smart Structures,* SPIE, **2427**, 300-309.

Lynch, C. S., 1996. The effect of uniaxial stress on the electro-mechanical response of 8/65/35 PLZT. *Acta Materialia* **44** (10): 4137-4148.

Lynch, C. S., 1998. On the development of multiaxial phenomenological constitutive laws for ferroelectric ceramics. *Journal of Intelligent Material Systems and Structures* **9**, 555-563.

Macki, J. W., Nistri, P. and Zecca. P., 1993. Mathematical models for hysteresis. *SIAM Review* **35**, 94-123.

McMeeking, R. M. and Hwang, S. C., 1997. On the potential energy of a piezoelectric inclusion and the criterion for ferroelectric switching. *Ferroelectrics* **200**, 151-173.

Morney, R. M., White, R. M. and Howe, R. T., 1989. Ultrasonic micromotors. *Proceedings of the IEEE Ultrrasonics Symposium,* 745-748. Montreal, 1989.

Nakagawa, T., Yamaguchi, J., Okugama, M. and Hamakawa, Y., 1982. Preparation of PbTiO/sub 3/ ferroelectric thin film by chemical vapor deposition. *Japanese Journal of Applied Physics Part 2–Letters* **21** (10): 655-656.

Ong, R., 2001. Masters Thesis, Department of Materials Science and Engineering, University of Illinois, Urbana, IL.

Polla, D. L., Muller, R. S. and White, R. M., 1986. Integrated multisensor chip. *IEEE Electron Device Letters* **EDL-7**: 254-256.

Saito, Y. and Hori, S., 1994. Acoustic emission and domain switching in tetragonal lead zirconate titanate ceramics. *Japanese Journal of Applied Physics Part 1* **33** (9B): 5555-5558.

Sengupta, S. S., Park, S. M., Payne, D. A. and Allen, L. H., 1998. Origins and evolution of stress development in sol-gel derived thin layers and multi deposited coatings of lead titanate. *Journal of Applied Physics* **83** (4): 2291-2296.

Spierings, G. A. C. M., G. J. M. Dormans, W. G. J. Moors, and M. J. E. Ulenaers, 1995. Stresses in Pt/Pb(Zr,Ti)O_3/Pt thin-film stacks for integrated ferroelectric capacitors, *Journal of Applied Physics* **78** (3), pp. 1926-1933.

Surowiak, Z., Zajosz, H. and Dytry, R., 1978. A system for deposition of ferroelectric substances by radio-frequency sputtering. *Thin Solid Films* **51**: 359-362.

Tuttle, B. A., Voigt, J. A., Garino, T. J., Goodnow, D. C., Schwartz, R. W., Lamppa, D. L., Headley, T. J. and Eatough, M. O., 1992. Chemically prepared Pb(Zr,Ti)O_3 thin films: the effects of orientation and stress. Proceedings of the Eighth IEEE International Symposium on Applications of Ferroelectrics, 344-348. New York.

Wenzel, S. W. and White, R. M., 1988. A multisensor employing an ultrasonic Lamb-wave oscillator. *IEEE Transactions on Electron* **35** (6)**:** 735-743.

Zhang, Q. M., Jang, S. J. and Cross, L. E., 1989. High-frequency strain response in ferroelectrics and its measurement using a modified Mach-Zehnder interferometer. *Journal of Applied Physics* **65** (7): 2807-2813.

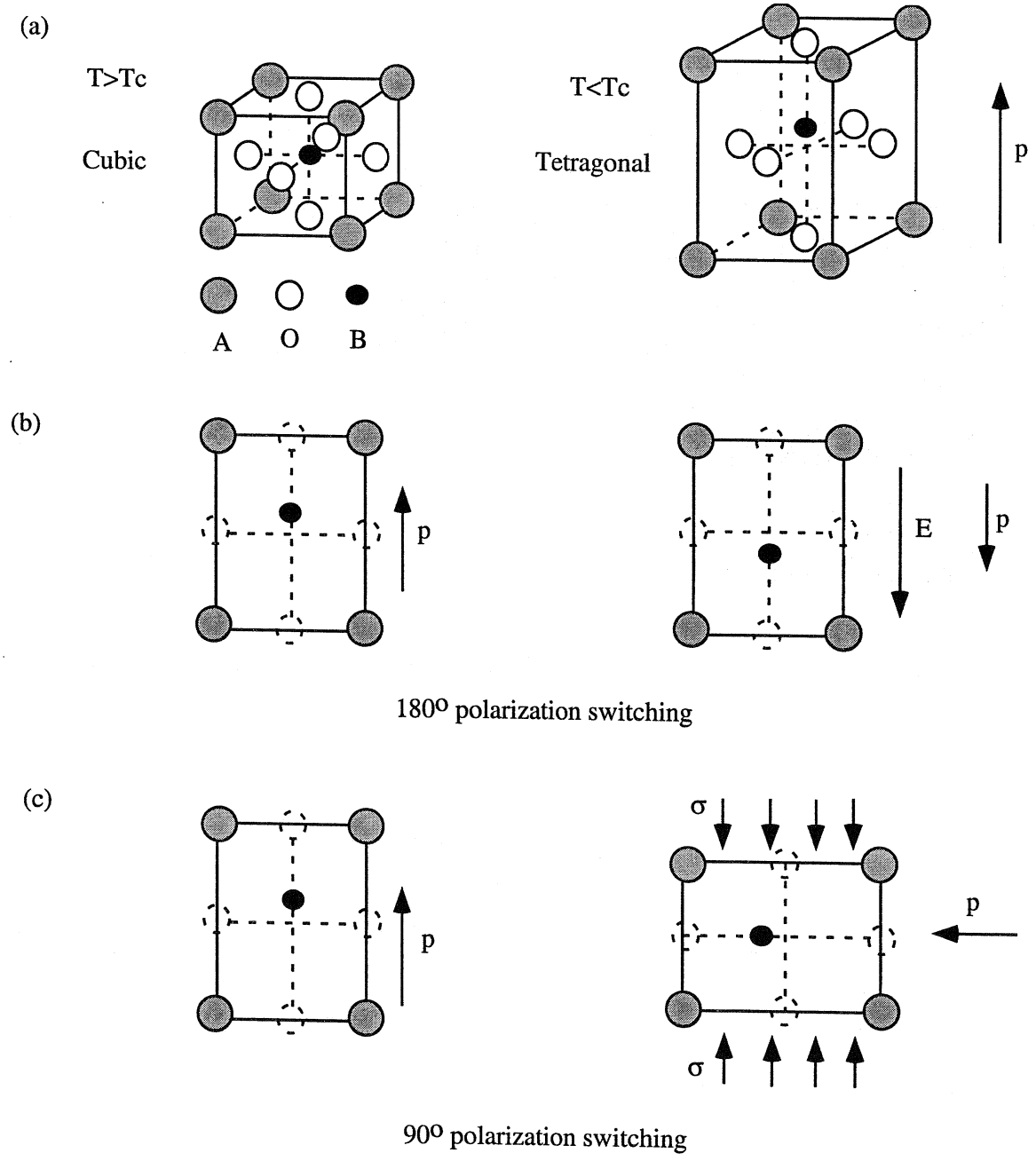

Fig. 1. (a) The cubic to tetragonal transition of an ABO_3 perovskite structure.
(b) 180° polarization switching induced by an electric field above the coercive field.
(c) 90° polarization switching induced by a compressive stress above the coercive stress.

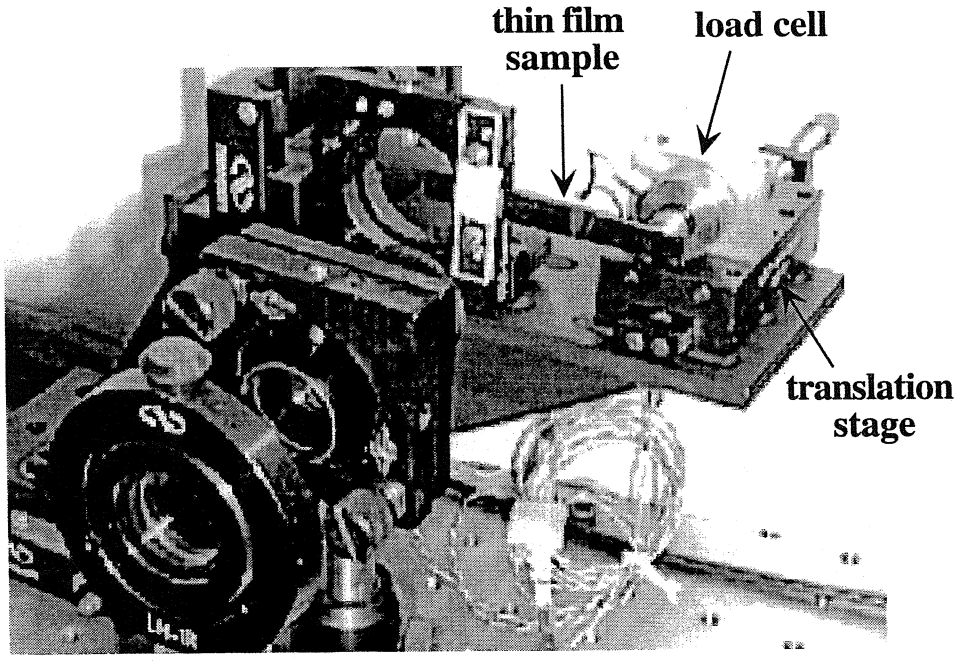

Fig. 2. Experimental apparatus for applying bending loads to thin-film ferroelectric samples during interferometric measurements.

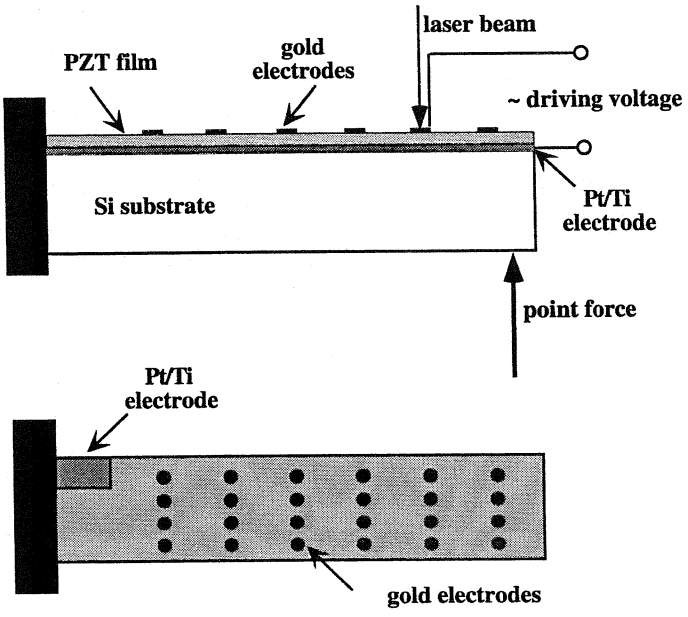

Fig. 3. Schematic of the beam sample used in the interferometric measurements.

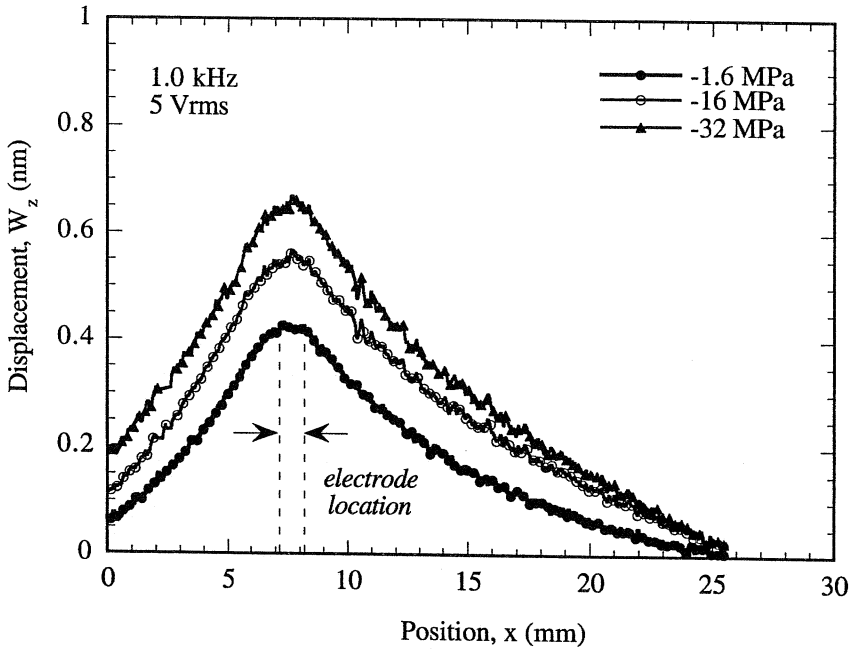

Fig. 4. Out-of-plane displacement profile of a PZT/Si cantilever beam at different applied compressive stress levels.

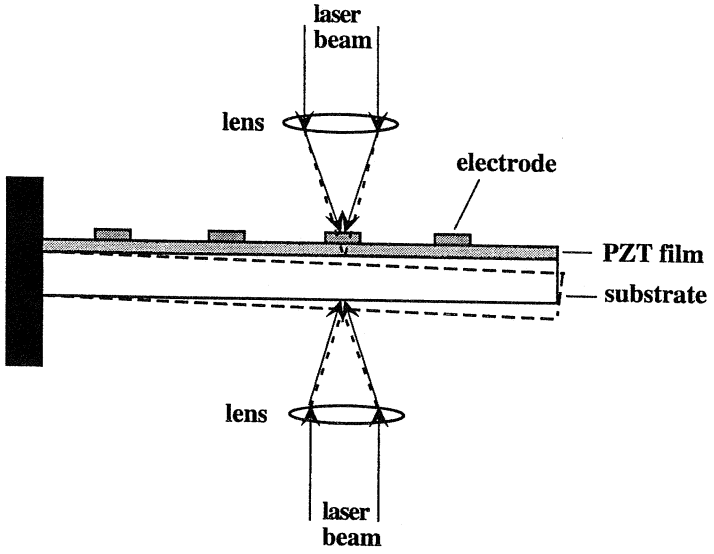

Fig. 5. Schematic of a sample in the double-beam interferometer.

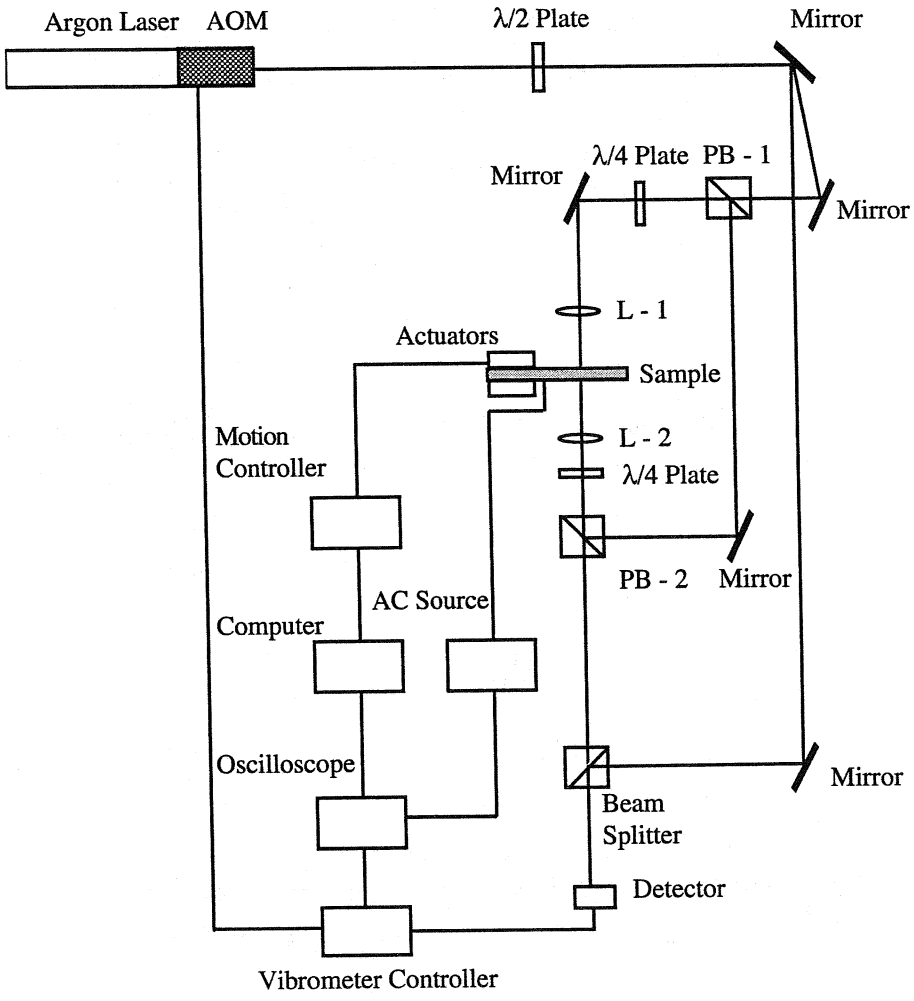

Fig. 6. Double-beam laser-Doppler hetrodyne interferometer.

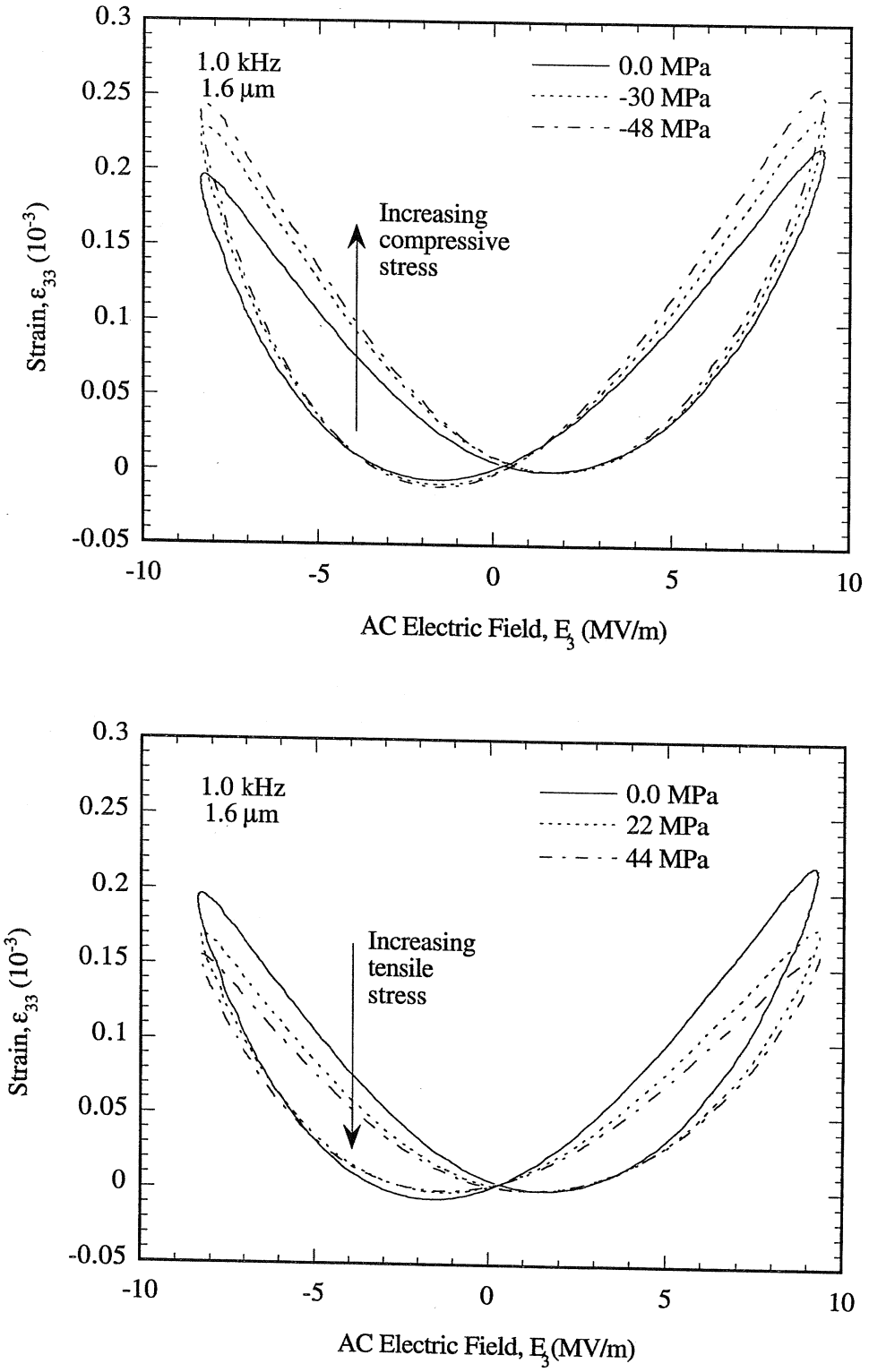

Fig. 7. Field-induced strains in 1.6 μm thick PZT (52/48) film under (a) increasing compressive bending load, (b) increasing tensile bending load.

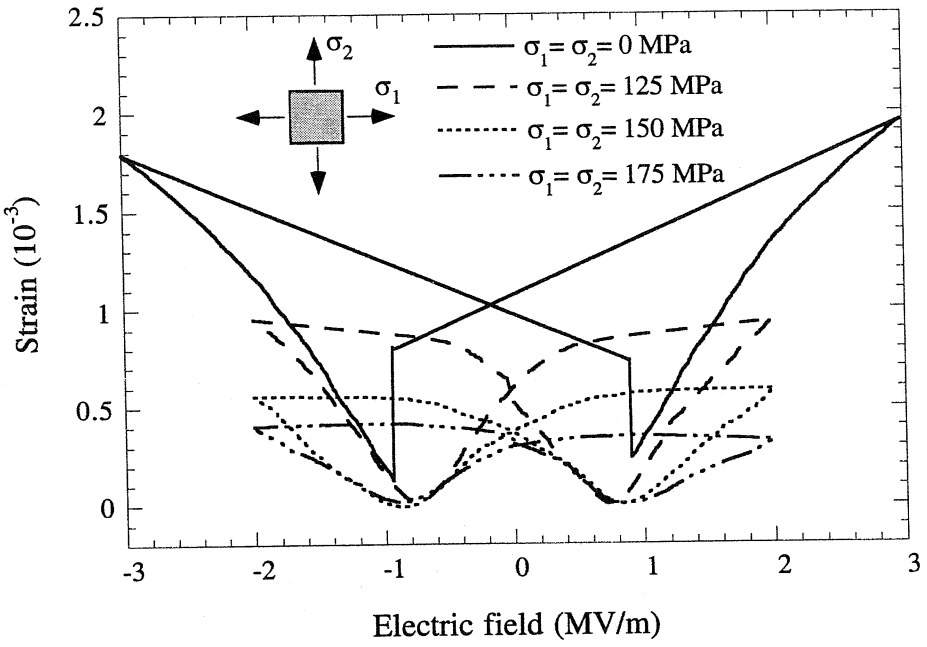

Fig. 8. Simulated longitudinal strain vs electric field hysteresis loops for tetragonal PZT (53/47) with preferred orientation under transverse biaxial tensile stress.

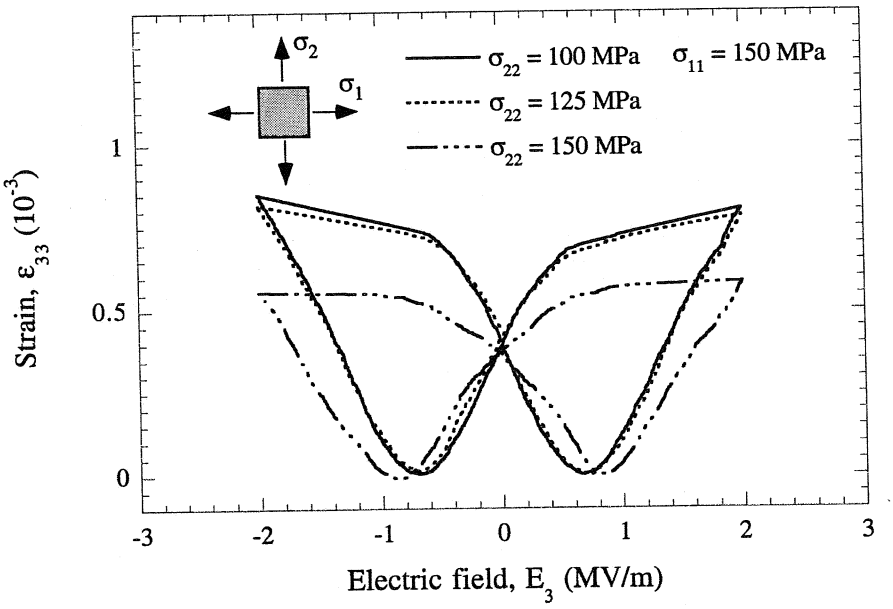

Fig. 9. Simulated longitudinal strain vs electric field hysteresis loops for tetragonal PZT (53/47) under transverse biaxial tensile stress with reduction in stress in one direction.

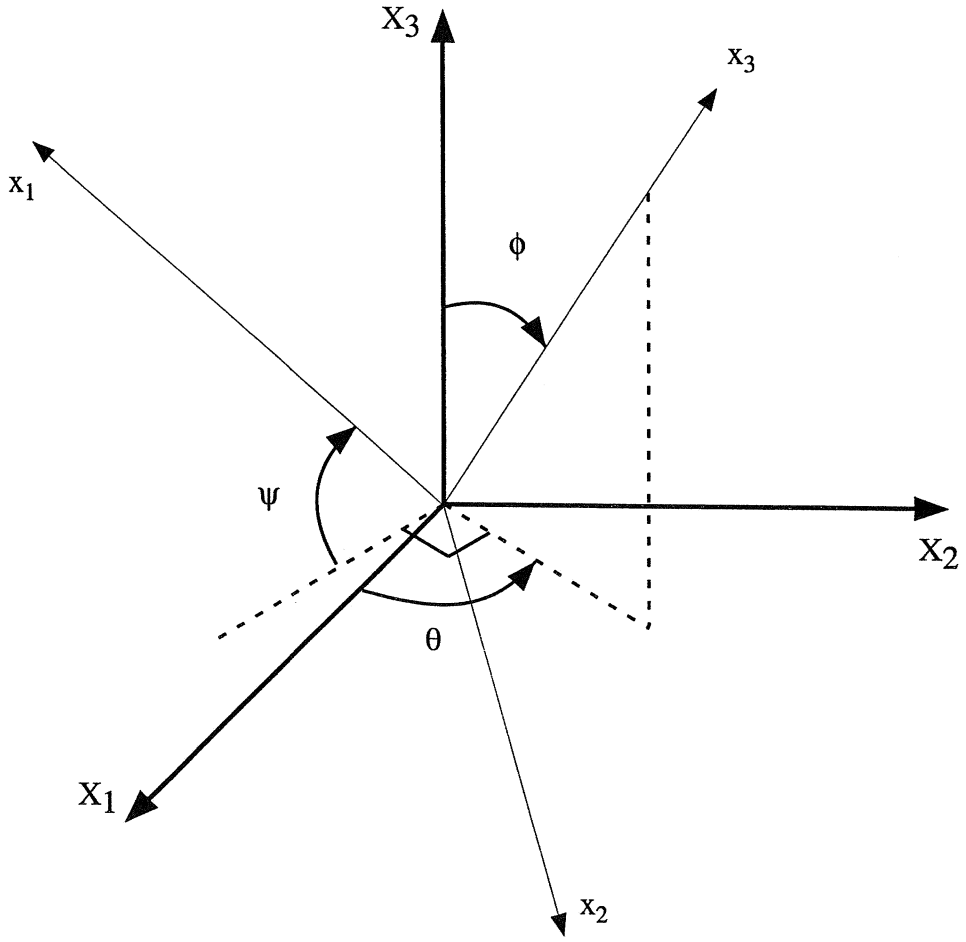

Fig. 10. Definition of the Euler angles in the coordinate transformation.

Table 1. Material constants used in the numerical simulation of PZT (53/47).

Young's modulus Y [N m^{-2}]	72×10^{9}
Poisson's ration ν	0.3
Dielectric permittivity κ [F m^{-1}]	1.76×10^{-8}
Piezoelectric coefficient d_{33} [m V^{-1}]	1.0×10^{-9}
Spontaneous strain e_0	0.003
Spontaneous polarization P_0 [C m^{-2}]	0.4
Coercive field for 90° switching $E_0^{\bar{9}0}$ [V m^{-1}]	0.4×10^{6}
Coercive field for 180° switching $E_0^{\bar{1}80}$ [V m^{-1}]	1.0×10^{6}
Weighting parameter α	1.0
Effective Young's modulus $\bar{Y}$ [N m^{-2}]	25×10^{9}
Effective dielectric permittivity $\bar{\kappa}$ [F m^{-1}]	2.5×10^{-7}

List of Recent TAM Reports

No.	Authors	Title	Date
891	Kim, K. C., and R. J. Adrian	Very large-scale motion in the outer layer—*Physics of Fluids* **2**, 417–422 (1999)	Oct. 1998
892	Fujisawa, N., and R. J. Adrian	Three-dimensional temperature measurement in turbulent thermal convection by extended range scanning liquid crystal thermometry—*Journal of Visualization* **1**, 355–364 (1999)	Oct. 1998
893	Shen, A. Q., E. Fried, and S. T. Thoroddsen	Is segregation-by-particle-type a generic mechanism underlying finger formation at fronts of flowing granular media?—*Particulate Science and Technology* **17**, 141–148 (1999)	Oct. 1998
894	Shen, A. Q.	Mathematical and analog modeling of lava dome growth	Oct. 1998
895	Buckmaster, J. D., and M. Short	Cellular instabilities, sub-limit structures, and edge-flames in premixed counterflows—*Combustion Theory and Modeling* **3**, 199–214 (1999)	Oct. 1998
896	Harris, J. G.	*Elastic waves*—Part of a book to be published by Cambridge University Press	Dec. 1998
897	Paris, A. J., and G. A. Costello	Cord composite cylindrical shells—*Journal of Applied Mechanics* **67**, 117–127 (2000)	Dec. 1998
898	Students in TAM 293–294	Thirty-fourth student symposium on engineering mechanics (May 1997), J. W. Phillips, coordinator: Selected senior projects by M. R. Bracki, A. K. Davis, J. A. (Myers) Hommema, and P. D. Pattillo	Dec. 1998
899	Taha, A., and P. Sofronis	A micromechanics approach to the study of hydrogen transport and embrittlement—*Engineering Fracture Mechanics* **68**, 803–837 (2001)	Jan. 1999
900	Ferney, B. D., and K. J. Hsia	The influence of multiple slip systems on the brittle–ductile transition in silicon—*Materials Science Engineering A* **272**, 422–430 (1999)	Feb. 1999
901	Fried, E., and A. Q. Shen	Supplemental relations at a phase interface across which the velocity and temperature jump—*Continuum Mechanics and Thermodynamics* **11**, 277–296 (1999)	Mar. 1999
902	Paris, A. J., and G. A. Costello	Cord composite cylindrical shells: Multiple layers of cords at various angles to the shell axis	Apr. 1999
903	Ferney, B. D., M. R. DeVary, K. J. Hsia, and A. Needleman	Oscillatory crack growth in glass—*Scripta Materialia* **41**, 275–281 (1999)	Apr. 1999
904	Fried, E., and S. Sellers	Microforces and the theory of solute transport—*Zeitschrift für angewandte Mathematik und Physik* **51**, 732–751 (2000)	Apr. 1999
905	Balachandar, S., J. D. Buckmaster, and M. Short	The generation of axial vorticity in solid-propellant rocket-motor flows—*Journal of Fluid Mechanics* (submitted)	May 1999
906	Aref, H., and D. L. Vainchtein	The equation of state of a foam—*Physics of Fluids* **12**, 23–28 (2000)	May 1999
907	Subramanian, S. J., and P. Sofronis	Modeling of the interaction between densification mechanisms in powder compaction—*International Journal of Solids and Structures*, in press (2000)	May 1999
908	Aref, H., and M. A. Stremler	Four-vortex motion with zero total circulation and impulse—*Physics of Fluids* **11**, 3704-3715	May 1999
909	Adrian, R. J., K. T. Christensen, and Z.-C. Liu	On the analysis and interpretation of turbulent velocity fields—*Experiments in Fluids* **29**, 275–290 (2000)	May 1999
910	Fried, E., and S. Sellers	Theory for atomic diffusion on fixed and deformable crystal lattices—*Journal of Elasticity* **59**, 67–81 (2000)	June 1999
911	Sofronis, P., and N. Aravas	Hydrogen induced shear localization of the plastic flow in metals and alloys—*European Journal of Mechanics/A Solids* (submitted)	June 1999

List of Recent TAM Reports (cont'd)

No.	Authors	Title	Date
912	Anderson, D. R., D. E. Carlson, and E. Fried	A continuum-mechanical theory for nematic elastomers—*Journal of Elasticity* **56**, 33–58 (1999)	June 1999
913	Riahi, D. N.	High Rayleigh number convection in a rotating melt during alloy solidification—*Recent Developments in Crystal Growth Research* **2**, 211–222 (2000)	July 1999
914	Riahi, D. N.	Buoyancy driven flow in a rotating low Prandtl number melt during alloy solidification—*Current Topics in Crystal Growth Research* **5**, 151–161 (2000)	July 1999
915	Adrian, R. J.	On the physical space equation for large-eddy simulation of inhomogeneous turbulence—*Physics of Fluids* (submitted)	July 1999
916	Riahi, D. N.	Wave and vortex generation and interaction in turbulent channel flow between wavy boundaries—*Journal of Mathematical Fluid Mechanics* (submitted)	July 1999
917	Boyland, P. L., M. A. Stremler, and H. Aref	Topological fluid mechanics of point vortex motions	July 1999
918	Riahi, D. N.	Effects of a vertical magnetic field on chimney convection in a mushy layer—*Journal of Crystal Growth* **216**, 501–511 (2000)	Aug. 1999
919	Riahi, D. N.	Boundary mode–vortex interaction in turbulent channel flow over a non-wavy rough wall—*Proceedings of the Royal Society of London A* (submitted)	Sept. 1999
920	Block, G. I., J. G. Harris, and T. Hayat	Measurement models for ultrasonic nondestructive evaluation—*IEEE Transactions on Ultrasonics, Ferroelectrics, and Frequency Control* **47**, 604–611 (2000)	Sept. 1999
921	Zhang, S., and K. J. Hsia	Modeling the fracture of a sandwich structure due to cavitation in a ductile adhesive layer—*Journal of Applied Mechanics* (submitted)	Sept. 1999
922	Nimmagadda, P. B. R., and P. Sofronis	Leading order asymptotics at sharp fiber corners in creeping-matrix composite materials	Oct. 1999
923	Yoo, S., and D. N. Riahi	Effects of a moving wavy boundary on channel flow instabilities—*Theoretical and Computational Fluid Dynamics* (submitted)	Nov. 1999
924	Adrian, R. J., C. D. Meinhart, and C. D. Tomkins	Vortex organization in the outer region of the turbulent boundary layer—*Journal of Fluid Mechanics* **422**, 1–53 (2000)	Nov. 1999
925	Riahi, D. N., and A. T. Hsui	Finite amplitude thermal convection with variable gravity—*International Journal of Mathematics and Mathematical Sciences* **25**, 153–165 (2001)	Dec. 1999
926	Kwok, W. Y., R. D. Moser, and J. Jiménez	A critical evaluation of the resolution properties of *B*-spline and compact finite difference methods—*Journal of Computational Physics* (submitted)	Feb. 2000
927	Ferry, J. P., and S. Balachandar	A fast Eulerian method for two-phase flow—*International Journal of Multiphase Flow*, in press (2000)	Feb. 2000
928	Thoroddsen, S. T., and K. Takehara	The coalescence–cascade of a drop—*Physics of Fluids* **12**, 1257–1265 (2000)	Feb. 2000
929	Liu, Z.-C., R. J. Adrian, and T. J. Hanratty	Large-scale modes of turbulent channel flow: Transport and structure—*Journal of Fluid Mechanics* (submitted)	Feb. 2000
930	Borodai, S. G., and R. D. Moser	The numerical decomposition of turbulent fluctuations in a compressible boundary layer—*Theoretical and Computational Fluid Dynamics* (submitted)	Mar. 2000
931	Balachandar, S., and F. M. Najjar	Optimal two-dimensional models for wake flows—*Physics of Fluids*, in press (2000)	Mar. 2000
932	Yoon, H. S., K. V. Sharp, D. F. Hill, R. J. Adrian, S. Balachandar, M. Y. Ha, and K. Kar	Integrated experimental and computational approach to simulation of flow in a stirred tank—*Chemical Engineering Sciences* (submitted)	Mar. 2000

List of Recent TAM Reports (cont'd)

No.	Authors	Title	Date
933	Sakakibara, J., Hishida, K., and W. R. C. Phillips	On the vortical structure in a plane impinging jet—*Journal of Fluid Mechanics* **434**, 273–300 (2001)	Apr. 2000
934	Phillips, W. R. C.	Eulerian space–time correlations in turbulent shear flows	Apr. 2000
935	Hsui, A. T., and D. N. Riahi	Onset of thermal–chemical convection with crystallization within a binary fluid and its geological implications—*Geochemistry, Geophysics, Geosystems*, in press (2001)	Apr. 2000
936	Cermelli, P., E. Fried, and S. Sellers	Configurational stress, yield, and flow in rate-independent plasticity—*Proceedings of the Royal Society of London A* **457**, 1447–1467 (2001)	Apr. 2000
937	Adrian, R. J., C. Meneveau, R. D. Moser, and J. J. Riley	Final report on 'Turbulence Measurements for Large-Eddy Simulation' workshop	Apr. 2000
938	Bagchi, P., and S. Balachandar	Linearly varying ambient flow past a sphere at finite Reynolds number—Part 1: Wake structure and forces in steady straining flow	Apr. 2000
939	Gioia, G., A. DeSimone, M. Ortiz, and A. M. Cuitiño	Folding energetics in thin-film diaphragms	Apr. 2000
940	Chaïeb, S., and G. H. McKinley	Mixing immiscible fluids: Drainage induced cusp formation	May 2000
941	Thoroddsen, S. T., and A. Q. Shen	Granular jets	May 2000
942	Riahi, D. N.	Non-axisymmetric chimney convection in a mushy layer under a high-gravity environment—In *Centrifugal Materials Processing* (L. L. Regel and W. R. Wilcox, eds.), in press (2000)	May 2000
943	Christensen, K. T., S. M. Soloff, and R. J. Adrian	PIV Sleuth: Integrated particle image velocimetry interrogation/validation software	May 2000
944	Wang, J., N. R. Sottos, and R. L. Weaver	Laser induced thin film spallation—*Experimental Mechanics* (submitted)	May 2000
945	Riahi, D. N.	Magnetohydrodynamic effects in high gravity convection during alloy solidification—In *Centrifugal Materials Processing* (L. L. Regel and W. R. Wilcox, eds.), in press (2000)	June 2000
946	Gioia, G., Y. Wang, and A. M. Cuitiño	The energetics of heterogeneous deformation in open-cell solid foams	June 2000
947	Kessler, M. R., and S. R. White	Self-activated healing of delamination damage in woven composites—*Composites A: Applied Science and Manufacturing* **32**, 683–699 (2001)	June 2000
948	Phillips, W. R. C.	On the pseudomomentum and generalized Stokes drift in a spectrum of rotational waves—*Journal of Fluid Mechanics* **430**, 209–229 (2001)	July 2000
949	Hsui, A. T., and D. N. Riahi	Does the Earth's nonuniform gravitational field affect its mantle convection?—*Physics of the Earth and Planetary Interiors* (submitted)	July 2000
950	Phillips, J. W.	Abstract Book, 20th International Congress of Theoretical and Applied Mechanics (27 August – 2 September, 2000, Chicago)	July 2000
951	Vainchtein, D. L., and H. Aref	Morphological transition in compressible foam—*Physics of Fluids* **13**, 2152–2160 (2001)	July 2000
952	Chaïeb, S., F. Sato-Matsuo, and T. Tanaka	Shrinking-induced instabilities in gels	July 2000
953	Riahi, D. N., and A. T. Hsui	A theoretical investigation of high Rayleigh number convection in a nonuniform gravitational field—*Acta Mechanica* (submitted)	Aug. 2000
954	Riahi, D. N.	Effects of centrifugal and Coriolis forces on a hydromagnetic chimney convection in a mushy layer—*Journal of Crystal Growth*, in press (2001)	Aug. 2000

List of Recent TAM Reports (cont'd)

No.	Authors	Title	Date
955	Fried, E.	An elementary molecular-statistical basis for the Mooney and Rivlin–Saunders theories of rubber-elasticity—*Journal of the Mechanics and Physics of Solids*, in press (2001)	Sept. 2000
956	Phillips, W. R. C.	On an instability to Langmuir circulations and the role of Prandtl and Richardson numbers—*Journal of Fluid Mechanics*, in press (2001)	Sept. 2000
957	Chaïeb, S., and J. Sutin	Growth of myelin figures made of water soluble surfactant—Proceedings of the 1st Annual International IEEE–EMBS Conference on Microtechnologies in Medicine and Biology (October 2000, Lyon, France), 345–348	Oct. 2000
958	Christensen, K. T., and R. J. Adrian	Statistical evidence of hairpin vortex packets in wall turbulence—*Journal of Fluid Mechanics* **431**, 433–443 (2001)	Oct. 2000
959	Kuznetsov, I. R., and D. S. Stewart	Modeling the thermal expansion boundary layer during the combustion of energetic materials—*Combustion and Flame*, in press (2001)	Oct. 2000
960	Zhang, S., K. J. Hsia, and A. J. Pearlstein	Potential flow model of cavitation-induced interfacial fracture in a confined ductile layer—*Journal of the Mechanics and Physics of Solids* (submitted)	Nov. 2000
961	Sharp, K. V., R. J. Adrian, J. G. Santiago, and J. I. Molho	Liquid flows in microchannels—Chapter 6 of *CRC Handbook of MEMS* (M. Gad-el-Hak, ed.) (2001)	Nov. 2000
962	Harris, J. G.	Rayleigh wave propagation in curved waveguides—*Wave Motion*, in press (2001)	Jan. 2001
963	Dong, F., A. T. Hsui, and D. N. Riahi	A stability analysis and some numerical computations for thermal convection with a variable buoyancy factor—*Geophysical and Astrophysical Fluid Dynamics* (submitted)	Jan. 2001
964	Phillips, W. R. C.	Langmuir circulations beneath growing or decaying surface waves—*Journal of Fluid Mechanics* (submitted)	Jan. 2001
965	Bdzil, J. B., D. S. Stewart, and T. L. Jackson	Program burn algorithms based on detonation shock dynamics—*Journal of Computational Physics* (submitted)	Jan. 2001
966	Bagchi, P., and S. Balachandar	Linearly varying ambient flow past a sphere at finite Reynolds number: Part 2—Equation of motion—*Journal of Fluid Mechanics* (submitted)	Feb. 2001
967	Cermelli, P., and E. Fried	The evolution equation for a disclination in a nematic fluid—*Proceedings of the Royal Society A* (submitted)	Apr. 2001
968	Riahi, D. N.	Effects of rotation on convection in a porous layer during alloy solidification—Chapter in *Transport Phenomena in Porous Media* (D. B. Ingham and I. Pop, eds.), Oxford: Elsevier Science (2001)	Apr. 2001
969	Damljanovic, V., and R. L. Weaver	Elastic waves in cylindrical waveguides of arbitrary cross section—*Journal of Sound and Vibration* (submitted)	May 2001
970	Gioia, G., and A. M. Cuitiño	Two-phase densification of cohesive granular aggregates	May 2001
971	Subramanian, S. J., and P. Sofronis	Calculation of a constitutive potential for isostatic powder compaction—*International Journal of Mechanical Sciences* (submitted)	June 2001
972	Sofronis, P., and I. M. Robertson	Atomistic scale experimental observations and micromechanical/continuum models for the effect of hydrogen on the mechanical behavior of metals—*Philosophical Magazine* (submitted)	June 2001
973	Pushkin, D. O., and H. Aref	Self-similarity theory of stationary coagulation—*Physics of Fluids* (submitted)	July 2001
974	Lian, L., and N. R. Sottos	Stress effects in ferroelectric thin films—*Journal of the Mechanics and Physics of Solids* (submitted)	Aug. 2001